Gas-Phase Dissociation Reactions of Protonated Saxitoxin and Neosaxitoxin

Lekha Sleno and Dietrich A. Volmer
Institute for Marine Biosciences, National Research Council, Halifax, Nova Scotia, Canada

Borislav Kovačević and Zvonimir B. Maksić
Quantum Chemistry Group, Rudjer Bošković Institute, Zagreb, Croatia

The aim of this study was to investigate the behavior of the protonated paralytic shellfish poisons saxitoxin (STX) and neosaxitoxin (NEO) in the gas-phase after ion activation using different tandem mass spectrometry techniques. STX and NEO belong to a group of neurotoxins produced by several strains of marine dinoflagellates. Their chemical structures are based on a tetrahydropurine skeleton to which a 5-membered ring is fused. STX and NEO only vary in their substituent at N-1, with STX carrying hydrogen and NEO having a hydroxyl group at this position. The collision-induced dissociation (CID) spectra exhibited an unusually rich variety and abundance of species due to the large number of functional groups within the small skeletal structures. Starting with triple-quadrupole CID spectra as templates, linked ion-trap MS^n data were added to provide tentative dissociation schemes. Subsequent high-resolution FTICR experiments gave exact mass data for product ions formed via infrared multiphoton dissociation (IRMPD) from which elemental formulas were derived. Calculations of proton affinities of STX and NEO suggested that protonation took place at the guanidinium group in the pyrimidine ring for both molecules. Most of the observed parallel and consecutive fragmentations could be rationalized through neutral losses of H_2O, NH_3, CO, CO_2, CH_2O and different isocyanate, ketenimine and diimine species, many of which were similar for STX and NEO. Several exceptions, however, were noted and differences could be readily correlated with reactions involving NEO's additional hydroxyl group. A few interesting variations between CID and IRMPD spectra are also highlighted in this paper. (J Am Soc Mass Spectrom 2004, 15, 462–477) © 2004 American Society for Mass Spectrometry

Paralytic shellfish poisons (PSPs) are a group of over 20 neurotoxins produced by several strains of marine dinoflagellates, mostly from the genus *Alexandrium* [1]. The primary sources of PSP toxins are harmful algal blooms ("red tides" [2]) in the oceans, occurring in different climate zones. Shellfish grazing on these algae cause bioaccumulation of these toxins. The subsequent occurrence of PSPs in shellfish is of great concern, owing to the highly toxic properties that these compounds exhibit in humans [3]. Studies have shown that PSP toxins selectively block Na^+ channels on excitable membranes, thereby blocking the propagation of nerve and skeletal muscle action potentials [4–6] leading to characteristic neurological symptoms, such as circumoral paresthesia, followed by cerebellar syndromes, cranial nerve involvement, and motor paralysis including respiratory failure [7]. Nausea, vomiting, and diarrhea are also sometimes observed [8]. Occasionally, respiratory paralyses occur with fatal consequences [9].

The chemical structures of PSPs are based on a tetrahydropurine skeleton to which a 5-membered ring is fused. They contain a unique hydrated ketone stabilized by two electron-withdrawing guanidinium moieties. Scheme **1** illustrates the structures of two high-toxicity carbamate PSPs, which will be discussed in detail in this report. The wide variety of known PSP analogs originates from further transformations at N-1 (hydroxyl addition [10]), C-11 (hydroxysulfate addition [11]), and N-21 (sulfonate addition [12]). The large number and the highly toxic nature of some of the PSP analogs require effective monitoring tools to detect their presence in contaminated seafood for consumer protection. Many countries have established regulatory guidelines and set maximum allowable concentrations for seafood samples. For example, the European Union established a maximum amount of 80 μg per 100 g of edible flesh for molluscs [13].

The most widely used monitoring tool for PSP toxins is the mouse bioassay, since it generally works well with water-soluble PSPs [14]. It is flawed, however, with respect to its narrow dynamic range and its inherent variability that can exceed ±20% [15]. More importantly, because of ethical considerations, animal-

Published online February 3, 2004

Address reprint requests to Dr. D. Volmer, Institute for Marine Biosciences, National Research Council, 1411 Oxford Street, Halifax, Nova Scotia B3H 3Z1, Canada. E-mail: Dietrich.Volmer@nrc.ca

1044-0305/04/$30.00
doi:10.1016/j.jasms.2003.11.013

Received August 27, 2003
Revised November 19, 2003
Accepted November 19, 2003

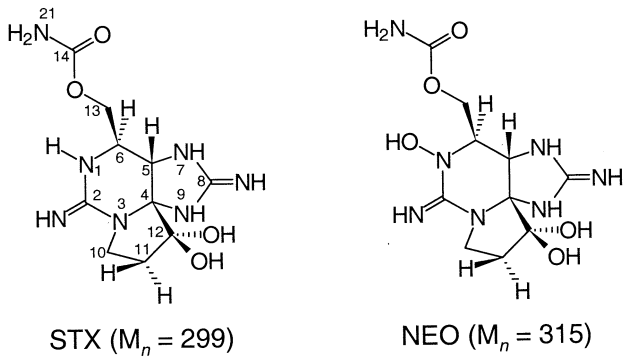

Scheme 1. Chemical structures and nominal molecular weights of saxitoxin (STX) and 1-*N*-hydroxysaxitoxin (neosaxitoxin, NEO).

based methods are no longer desirable. Consequently, alternative methodologies based on physicochemical substance properties are preferred for detection of PSPs.

To date, the majority of instrumental analytical methods for detection of PSP toxins have employed liquid chromatography (LC) or capillary electrophoresis (CE) with various detectors. It is not important, in the context of this paper, to summarize the numerous chromatographic studies on PSP toxins. Nevertheless, it should be briefly mentioned that PSPs are not easily analyzed by regular reversed-phase chromatography because of the high polarity of these molecules. Approaches such as ion-pairing or hydrophilic interaction LC, however, have overcome many of the problems associated with PSP separations. The present authors recommend reviews by Luckas [1] and Quilliam et al. [15–17], which summarize many excellent PSP chromatographic assays as well as a comprehensive publication by Thibault et al. [18] on CE analysis of PSPs.

The disadvantage of all non-specific CE or LC techniques is that subsequent confirmation is needed to ensure that the method does not yield any false responses. While enzyme immunoassay methods have been reported as screening tools for PSPs [19], only mass spectral analysis with a sufficient number of structurally significant product ions can provide unequivocal proof of the compound's presence in a sample [20]. Depending on the compound's structure, diagnostic product ions can be generated by classical electron impact (EI) mass spectrometry or, for soft ionization techniques, by tandem mass spectrometry (MS/MS).

Unfortunately, EI mass spectrometry cannot be implemented for PSPs because of their extraordinarily high polarities. A number of authors, however, have reported mass spectrometric assays based on soft ionization techniques, such as fast-atom bombardment (FAB) since the 1980s, with more sensitive and selective LC/MS methodologies dominating the field since the early 1990s. Nakamura and coworkers [21] used FAB to generate intact protonated molecules and adduct ions for saxitoxin (STX) with some fragmentation from the carbamoyl group. White et al. [22] described mass spectra with intact protonated molecules for 12 PSP toxins using FAB. The authors were also able to generate a series of diagnostic fragment ions in the mass range *m/z* 200–270 using mass-analyzed ion kinetic energy scans (MIKES) from the MH^+ ions. Mirocha et al. [23] reported an improved continuous flow FAB method for saxitoxin with a detection limit of 200 pg (signal-to-noise ratio = 11).

In recent years, electrospray ionization (ESI) has been the dominating technique in mass spectrometric determinations of PSPs [15–17, 24–27], although a recent paper by Hashimoto et al. demonstrated successful analysis of PSP analogs via sonic spray ionization (SSI) [28]. Furthermore, Andrinolo and coworkers [29] showed atmospheric-pressure chemical ionization (APCI) analysis of STX at low cone voltages with some fragment ions visible in the spectrum. The paper did not, however, indicate whether these fragment ions are due to in-source fragmentation reactions or thermal dissociations during vaporization. Wils and Hulst [30] made an interesting observation during thermospray LC/MS of STX. Using buffer ionization, the authors were able to generate MH^+ ions only when spraying acidic solutions (pH = 2) with additional abundant fragment ions present. No intact MH^+ ions were observed from regular ammonium acetate buffered solutions. Unfortunately, the APCI fragment ions reported by Andrinolo and coworkers [29] and the thermospray fragment ions by Wilst and Hulst [30] do not seem to match to any significant degree, and thus did not allow identification of potential thermal degradations during the ionization of PSPs.

The pioneering PSP research in the area of electrospray ionization analysis has been conducted in the groups of Thibault et al. [27, 31–33] and Quilliam et al. [15–17, 24, 34]. In their studies, the authors used CE and LC separations prior to pneumatically-assisted ESI. Detection limits as low as 30 pg were obtained for positive ions of several saxitoxin analogs [34]. Since then, many other groups have established LC/ESI assays for PSPs with equally good sensitivities, mainly utilizing single or triple-quadrupole mass spectrometers, although some authors have successfully established ESI methods on ion-trap [35], time-of-flight [36] and quadrupole time-of-flight instruments [25].

Unfortunately, only a very limited number of tandem mass spectrometry (MS/MS) analyses of PSP toxins have been described previously. No detailed information on the dissociation pathways of protonated PSP molecules in the gas-phase appears to be available in the scientific literature. A few authors have reported neutral loss and ring cleavage reactions from the protonated toxin molecules. For example, Pleasance and coworkers [31] not only obtained product ions from the carbamoyl side chain for STX and NEO after electrospray ionization and collision-induced dissociation (CID) of the MH^+ ions in a triple-quadrupole instrument but also several product ions from the cyclic portions of the molecules. The authors presumed that

these additional ions were due to cleavage reactions at various charge sites in the molecules, the mechanisms of which were not described. Buzy and coworkers [32] used electrospray MS/MS on a triple-quadrupole instrument and described abundant dissociations during CID analysis from protonated decarbamoyl-saxitoxin (dcSTX), decarbamoyl-neosaxitoxin (dcNEO) and several other PSP analogs. A few ion-trap tandem mass spectra were shown by Reyero et al. [35] for dcSTX and NEO but only one non-specific H_2O loss was observed for the molecules in their analyses. Andrinolo et al. [29] reported an unexpected in-source CID spectrum for STX at high cone voltages. The authors interpreted the solitary product ion at *m/z* 74 as a protonated guanidine fragment of STX.

The goal of this study was to investigate the behavior of PSPs after collisional activation in the gas-phase. It was not the intention to add yet another improved PSP analytical methodology to the numerous assays already present in the literature. Rather, a detailed mechanistic look at the dissociation of the protonated molecules and the identification of fragmentation pathways. A variety of MS/MS techniques were used throughout the study including collisional activation in triple-quadrupole and ion-trap instruments, as well as Fourier-transform ion cyclotron resonance (FTICR) infrared multiphoton dissociation (IRMPD). As far as we know, no detailed MS/MS study on PSPs is currently available in the literature. From a scientific point of view, this is unexpected, as these small molecules exhibit a surprisingly large variety of competing low energy dissociation pathways. The resulting product ion mass spectra exhibit an unusually rich variety and abundance of different ion species. The insight gained from this investigation is expected to be extremely valuable in the characterization of other PSP analogs as well in the identification of yet unknown toxins. In the present work, two different PSPs were chosen as representative test compounds, saxitoxin (MH^+ at *m/z* 300) and neosaxitoxin (MH^+ at *m/z* 316). These two molecules only differ in their substituent at N-1, with STX carrying hydrogen and NEO having a hydroxyl group at this position (Scheme **1**). As will be discussed, the subtle substitution difference causes several significant variations in the appearance of the product ion spectra of the protonated molecules.

Experimental

Chemicals and Standard Solutions

Reference standard solutions of saxitoxin (65 μmol·L^{-1} in $3{\cdot}10^{-3}$ *M* HCl) and neosaxitoxin (65 μmol·L^{-1} in $3{\cdot}10^{-3}$ *M* HCl) were obtained through IMB's Certified Reference Materials Program (Halifax, NS, Canada) and were diluted 40-fold in 50:50 (vol/vol) methanol/water (+0.1% formic acid) prior to infusion into the mass spectrometers. Formic acid, N_α-acetyl-Arg, Lys-Leu, Phe-Gly-Gly-Phe, and [Glu^1]-Fribrinopeptide were purchased from Sigma-Aldrich (Mississauga, ON, Canada). Methanol (Caledon, Georgetown, ON, Canada) and Milli-Q organic free water (Millipore, Bedford, MA) were used as solvents.

Electrospray Triple-Quadrupole and Ion-Trap Tandem Mass Spectrometry

Electrospray MS/MS and MS^n data were acquired on MDS-Sciex (Concord, ON, Canada) API 4000 triple-quadrupole and Agilent (San Jose, CA) 1100 LC/MSD SL ion-trap (IT) mass spectrometers in the positive ion mode. The sample solutions were introduced into the mass spectrometers via a Harvard (Holliston, MA) syringe pump at 5 μL·min^{-1}. The API 4000's orthogonal Turbo-V source was operated at a spray voltage of 5 kV and a declustering potential of 60 V. The heat injectors were heated to 450 °C. N_2 was used as the collision gas (CAD gas setting at 6) at a collision-offset voltage of 35 V. In MS/MS mode, Q1 and Q3 were set to unit resolution. The ion-trap instrument was operated at the following settings: capillary voltage, −4.5 kV; nebulizer, 45 psi; dry gas, 7 L·min^{-1}; dry temperature, 325 °C; trap target, 50,000; maximum scan time, 5 ms. The fragmentation voltage was set to between 1–5 V; it was also ramped during the CID experiments from 50 to 150% (SmartFrag). An isolation width of 2 u was used in all MS^n experiments.

FTICR-MS and IRMPD FTICR-MS/MS

Exact mass measurements were performed at NHMFL (Tallahassee, FL) with a 9.4 tesla QFTICR instrument. Sample and calibration solutions were introduced at 400 nL·min^{-1} from separate sprayers of a dual ESI source. Ions were transferred through a Chait-style atmosphere-to-vacuum interface [37] and accumulated within a linear octopole, modified for improved ion ejection along the z-axis [38]. Mass-selected calibration and sample ions were individually accumulated for 5 and 1 s, respectively. All ions were then transferred through an octopole ion guide to the ICR cell. Hanning apodization and one zero-fill were applied to all data prior to the fast Fourier-transform and magnitude calculation [39]. Frequency spectra were calibrated internally [40, 41] from the measured ICR frequencies of the calibration mixture ions at *m/z* 217.12952 (N_α-acetyl-Arg), *m/z* 260.19687 (Lys-Leu), and *m/z* 427.19760 (Phe-Gly-Gly-Phe). The spectrum was the sum of 50 time-domain transients (2 Mb data). In infrared multiphoton dissociation (IRMPD), product ion data were internally calibrated by tailoring the stored-waveform inverse Fourier transform (SWIFT) [42, 43] waveform to isolate precursor (STX, *m/z* 300; NEO, *m/z* 316) and Glu-Fib [M + 2H]$^{2+}$ (*m/z* 785.8) ions, followed by irradiation with a 40W CO_2 laser (150 ms; 90% laser power). Glu-Fib product ions at *m/z* 175.11893 (y_1), 246.15607 (y_2), and 333.18807 (y_3) were used for calibration. The generated

product ions were then subjected to chirp excitation and direct-mode broadband detection. Spectra represent the sum of 50 scans of 150 ms each (2 Mb data). For elemental formula assignments of product ions in IRMPD, the atom constraints for C, H, N, and O were set to the respective number of atoms in the precursor ion molecules ($C_{10}H_{18}N_7O_4$ for STX and $C_{10}H_{18}N_7O_5$ for NEO, respectively).

Computational Approach for Calculation of Absolute Proton Affinities

The theoretical framework [44–46] for calculating the absolute proton affinity (*APA*) in the gas-phase is given by:

$$APA(B_\alpha) = (\Delta E_{el})_\alpha + (\Delta E_{vib})_\alpha + (5/2)RT \quad (1)$$

$$(\Delta E_{el})_\alpha = E(B) - E(B_\alpha H)^+ \quad (2)$$

$$(\Delta E_{vib})_\alpha = E_{vib}(B) - E_{vib}(B_\alpha H)^+ \quad (3)$$

The base and its conjugate acid are denoted by B and BH^+, respectively, whereas α indicates the site of proton attack. Eqs 2 and 3 describe the electronic $(\Delta E_{el})_\alpha$ and vibrational $(\Delta E_{vib})_\alpha$ energy contributions to the proton affinity, respectively. The former includes the nuclear repulsion term. The latter (E_{vib}) involves the zero point vibrational energy at 0K and the temperature correction to 298K. The (5/2)RT contribution recovers the translational energy of the proton and the $\Delta(PV)$ term. The search of the Born-Oppenheimer energy hypersurfaces was performed with an efficient DFT (density functional theory)—B3LYP computational scheme [47] employing the 6-31G* basis set. The minima on the hypersurface, which correspond to equilibrium spatial structures, were verified by vibrational analyses at the same level. The resulting geometries were used in the final single point calculations utilizing the 6-311 + G** basis set, which is flexible enough to describe the nitrogen lone pair [48]. The full notation for the applied theoretical method is B3LYP/6-311 + G**//B3LYP/6-31G* + E_{vib}(B3LYP/6-31G*), which will be abbreviated from here on as B3LYP. All computations were carried out using the Gaussian 98 program package [49].

Results and Discussion

This study describes the dissociation behavior of electrosprayed PSP toxins in the gas-phase, after ion activation of the protonated molecules (MH^+). From a mass spectrometric standpoint, PSP analogs are very intriguing as they contain a large number of different functional groups within a rather small skeletal structure. They also exhibit multiple charge sites [50, 51] owing to the two guanidinium groups per molecule, and the possibility for extensive resonance stabilization of fragment ions after dissociation, thus making a wide variety of competing low energy dissociation pathways possible. As will be shown below, the resulting product ion mass spectra of PSPs exhibit an unusually rich variety and abundance of different ion species.

Saxitoxin (STX) and 1-*N*-hydroxy-saxitoxin (Neosaxitoxin, NEO) were chosen as representative PSP model compounds because of their uncommon solution-phase basicity variations among the guanidinium groups (the indices L and R are in used in the following text to distinguish between the left-hand [pyrimidine ring] and the right-hand [imidazoline ring] group). Both compounds are virtually identical in their skeletal structure including the fused 5-ring at N-3/C-4 and the carbamoyl group at C-6 (Scheme **1**). According to studies on the aqueous dissociation constants (p*K*a), the subtle substitution difference at N-1 of the pyrimidine guanidinium group, however, results in a significant change of p*K*a. While the guanidinium group in the imidazoline ring of NEO was reported to have a p*K*a value similar to that of STX (p*K*a(R) = 8.24 versus 8.65 [12, 50]), the additional −OH group of NEO at N-1 seems to significantly diminish the basicity of the imino nitrogen at C-2 of the pyrimidine ring in aqueous solutions. This can clearly be seen from the observed sharp drop of the p*K*a(L) values from 11.28 for STX to 6.75 for NEO [50, 51]. Shimizu [12] pointed out that p*K*a values for the imidazoline guanidinium groups of PSPs are significantly lower than usually observed for guanidinium compounds. Presumably this is a result of insufficient participation of N-7 in the guanidinium resonance, caused most likely by stereochemical strain of the 5-ring. It was of interest to see if similar basicity differences could be observed in the gas-phase and if and how they may affect the dissociation behavior of the protonated molecules with respect to the site of charge-retention and the availability of competing low-energy dissociation pathways.

In the following text, the main features of the CID spectra of STX and NEO in a triple-quadrupole (QqQ) instrument are summarized along with a subsequent comprehensive mapping of the precursor ion/product ion relationships by ion-trap (IT) MS^n analysis, to give tentative dissociation schemes of the important linked information in the CID spectra. Subsequently, elemental formulae assignments were made to the tentatively identified ion structures from exact mass measurements obtained by infrared multiphoton dissociation (IRMPD) FTICR-MS. Next, a detailed discussion of the proton affinities of the PSPs is presented. Finally, an in-depth description of the dissociation pathways and mechanisms concludes this paper.

Collisional Activation of the Protonated Molecules

Collisional activation of the protonated molecules was initially performed in a triple-quadrupole instrument. The product ion spectra of saxitoxin and neosaxitoxin after collisional activation of the MH^+ ions are shown in

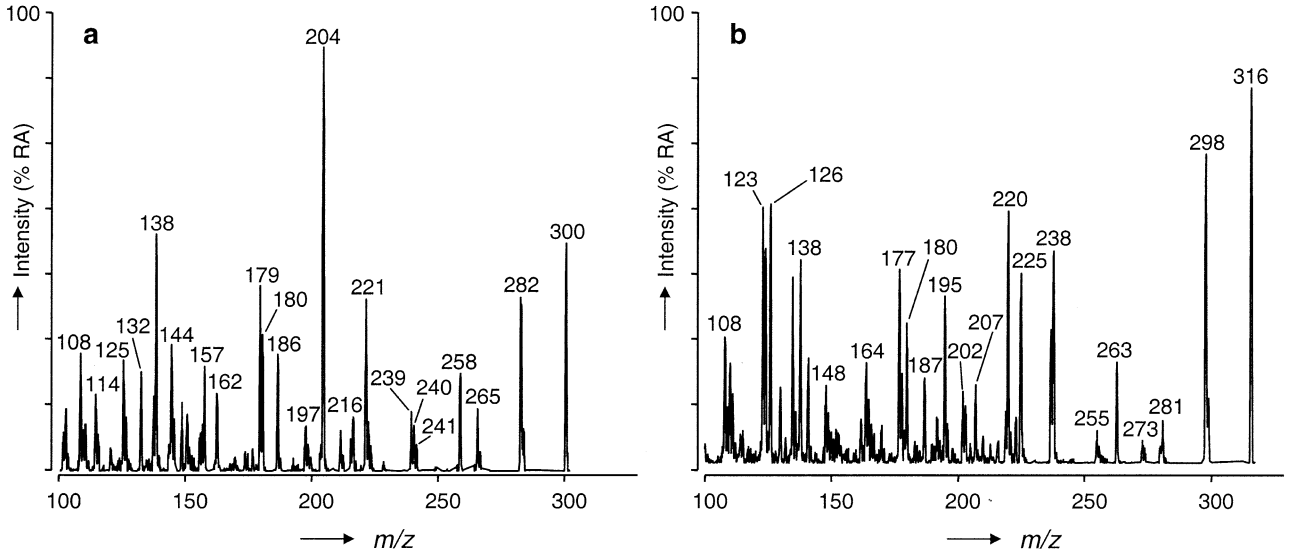

Figure 1. Triple-quadrupole CID spectra of STX and NEO after collisional activation of the MH^+ ions (*m/z* 300 and 316, respectively).

Figure 1a and b. As can be clearly observed, the two compounds exhibited an unusually large number of different product ions of significant abundance in the entire mass range investigated. When comparing the STX and NEO product ion spectra (Figure 1a and b), similarities between product ions of the two compounds can be readily noticed, indicating parallel dissociation mechanisms. A closer inspection, however, revealed several ion species formed by STX and NEO that were not the result of a simple 16 u mass shift due to the additional hydroxyl group of NEO at N-1. The fragmentation pathways and the mechanistic details are described in the last section of this paper.

This report only focuses on the mass range between *m/z* 137 and *m/z* 300/316 (MH^+, STX/NEO), because of the large number of abundant product ions. Nonetheless, the chosen *m/z* range covers up to six generations of consecutive reaction species (vide infra). Even with this additional restriction, the elucidation of dissociation pathways is difficult based on the QqQ data alone, as there is limited information on genealogical dissociation links in the triple-quadrupole CID spectra. Furthermore, consecutive dissociation reactions likely occur in the rich QqQ CID spectra of STX and NEO because extensive resonance stabilization of the STX and NEO product ions is possible. An additional complication in assigning unambiguous product ion structures and fragmentation pathways arose from the two possible protonation sites that both STX and NEO exhibit. While the solution-phase basicities (p*Ka*; vide supra) could be used to choose the most basic site for proton attachment (and thus a starting precursor ion structure for the elucidation of the fragmentation mechanisms), a computational calculation of the gas-phase proton affinities for STX and NEO was chosen to investigate potential differences between solution- and gas-phase behavior.

In order to establish tentative dissociation schemes for STX and NEO, genealogical maps of the linked precursor ion/product ion relationships were constructed from comprehensive ion-trap (IT) MS^n mapping experiments for many of the ion species observed in the QqQ CID experiments. As demonstrated by Strife et al. [52], ion-trap genealogical information can be added to QqQ CID spectra, where the QqQ spectra serve as initial templates for structure elucidations. We have taken a similar approach in this study. The resulting maps are summarized in Tables 1 and 2 for many of the ions from Figure 1a and b. By combining the CID data from QqQ and IT experiments, tentative linked dissociation schemes were generated for STX and NEO, as illustrated in Schemes **2** and **3**. Most of the observed consecutive fragmentation reactions can be rationalized through multiple neutral losses of H_2O, NH_3, CO, CO_2, CH_2O and different isocyanate, ketenimine and diimine species. The mechanistic details of these reactions are considered in the last section of this paper. Prior to explaining the exact dissociation mechanisms, it was necessary to confirm the identity of the product ions of the CID analyses by exact mass measurements.

Formula Assignment from Exact Mass Measurements

In a series of exact mass measurement experiments, elemental formula assignments were made to the tentative product ion structures observed in the QqQ CID spectra (Figure 1a and b) and the proposed dissociation pathways (Schemes **2** and **3**), to confirm the identity of the dissociation products. Infrared multiphoton disso-

Table 1. The relationships between several *n*th order precursor and product ions of STX (MH^+, *m/z* 300) from ion-trap MS^n CID experiments[a]

$$MH^+ \xrightarrow{MS^2} P_1^+ + N_1 \xrightarrow{MS^3} P_2^+ + N_2 \xrightarrow{MS^4} P_3^+ + N_3$$

MS^n where n=	2	3	3	4	3	4	3	3	3	4	3	4	4	QqQ (35V)
MH^+	300	300	300	300	300	300	300	300	300	300	300	300	300	300
P_1^+		282	266	282	258	258	240	239	221	282	204	282	258	
P_2^+				265		241				221		204	198	
Products	283													
	282													282
	266													
		265												265
		264												
														258
					241									
		240			240									
	239				239									239
								223						
							222	222						222
	221	**221**		221			221	221						221
	216													216
					215									
			205											
	204	**204**	204	**204**				204	**204**	**204**				**204**
		203		203										
					198	198	198							
					197		197	197						197
											194	194		
												187		
	186				186							186		186
		180			180	**180**	180	180						180
	179	179		179			**179**	**179**	179	179			**179**	179
			177											
			163											
		162		162			162			162	162	162		162
		161									161	161		
	157													157
						155								
							153			153				
			150	150			150				150	**150**		150
				148							**148**	**148**		148
		145												145
	144				**144**									144
		138					138							138
				137	137	137	137						137	137
	132													132
					126									126
							125							125
							114			114				114
													109	
														108

[a]Only ions with at least 10% relative abundance are listed. Ions highlighted in bold-face exhibited relative abundances of >95%.

ciation (IRMPD) analyses of the isolated protonated molecules of STX and NEO were carried out in the FTICR instrument. Most of the product ions of the QqQ CID analyses (Figure 1) also appeared in the IRMPD spectra and could therefore be used for deducing the elemental formulae. Recently, Xie and Lebrilla [53] made a similar observation when comparing IRMPD and CID methods for alkali metal-coordinated oligosaccharides, but noted a few minor, though not insignificant, differences due to the larger energy transferred during collisions. We also observed several interesting variations in our experiments; they are described in the final section of this paper.

Exact masses with mass uncertainties between −0.9 and +0.5 ppm were achieved for all of the STX and NEO product ions using internal mass calibration, as illustrated in Tables 3 and 4. (Note: Only ions also observed in the CID analyses on the QqQ instrument

Table 2. The relationships between several *n*th order precursor and product ions of NEO (MH^+, *m/z* 316) from ion-trap MS^n CID experiments[a]

$$MH^+ \xrightarrow{MS^2} P_1^+ + N_1 \xrightarrow{MS^3} P_2^+ + N_2 \xrightarrow{MS^4} P_3^+ + N_3$$

MS^n where n=	2	3	4	4	3	3	4	3	4	QqQ (35V)
MH^+	316	316	316	316	316	316	316	316	316	316
P_1^+		298	298	298	263	238	298	220	298	
P_2^+			281	263			237		220	
Products	**298**									**298**
		281								
		263	263							263
										238
	237	**237**								237
										225
						223				223
	220	**220**		**220**	**220**	**220**	**220**			**220**
						219	219			219
						210				
						209				
			207	207		207				207
							205		205	
		203	203					203	**203**	203
			202							202
										196
						195	195			195
								192	192	192
	187									187
		180								180
			179							
		178				178	**178**	178	178	178
	177	**177**				177	177		177	177
						170				170
							167			
		166				166	166	166		166
			165			165				165
		164	164					**164**	**164**	164
		162					162			162
			154							
		153					153			153
		152								152
			151							151
			150			150				150
										149
										148
							141			141
	138	138								**138**
			136							136
		135	135				135			135
							130			130
										126
						124	124			124
						123	123		123	123
			122							
							114			
										111
										110
										108

[a]Only ions with at least 10% relative abundance are listed. Ions highlighted in bold-face exhibited relative abundances of >95%.

are shown). As a result, only one possible elemental formula match for every fragment ion in the tables was obtained, thus establishing excellent confidence in the IRMPD FTICR-MS technique and in the identities of the proposed structures in Schemes **2** and **3**. Figure 2 illustrates a partial IRMPD FTICR spectrum of STX, exhibiting excellent peak shapes with resolving powers between 105,000 (*m/z* 283) and 215,000 (*m/z* 137). Simi-

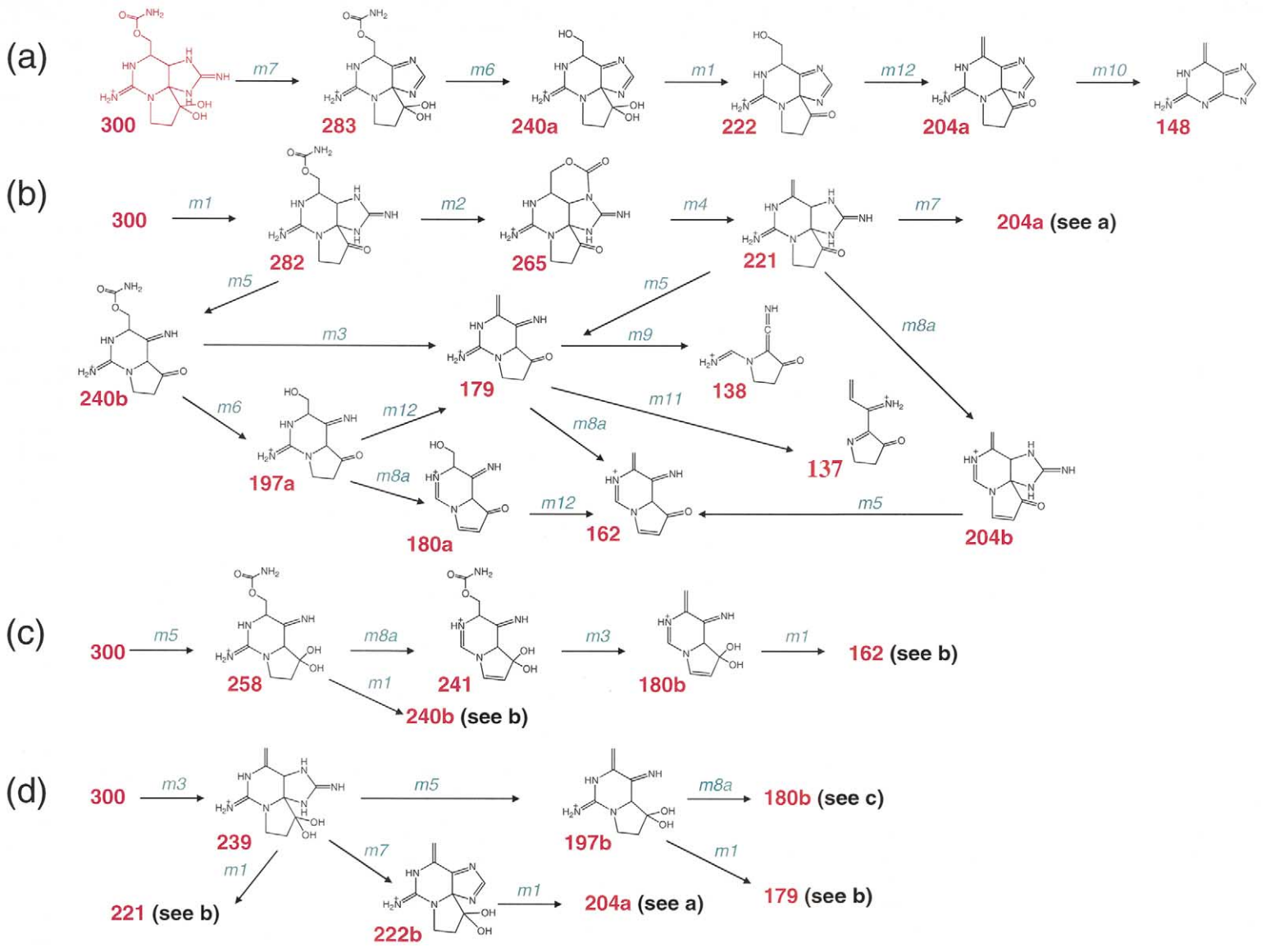

Scheme 2. Proposed principal dissociation reactions in triple-quadrupole CID analysis of the MH^+ ion of STX (*m/z* 300). (Parallel reactions of the MH^+ and $[MH - H_2O]^+$ ions are described by Pathways a–d. The reaction mechanisms ***m1–m18*** are summarized in Scheme 5).

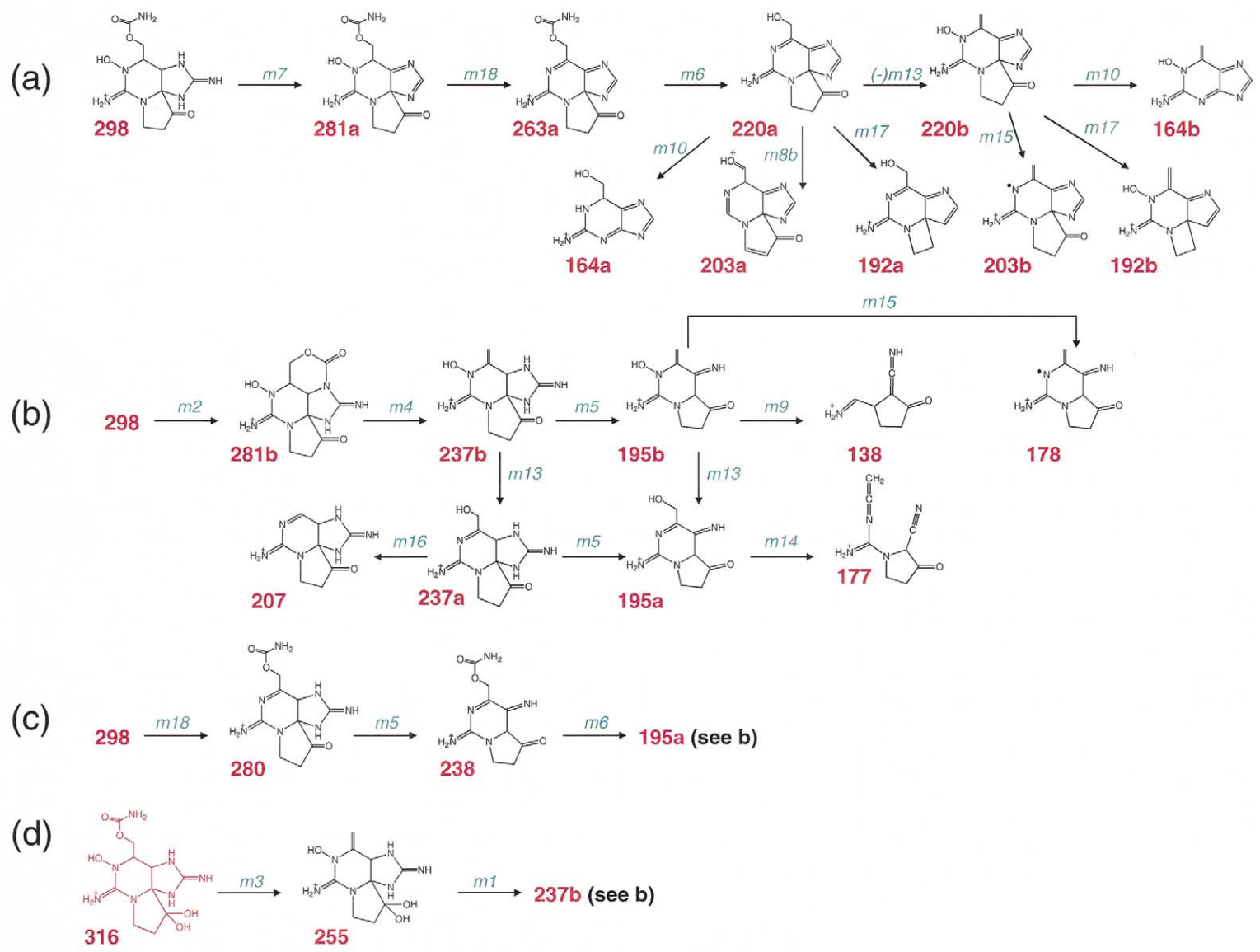

Scheme 3. Proposed principal dissociation reactions in triple-quadrupole CID analysis of the MH^+ ion of NEO (*m/z* 316). (Parallel reactions of the MH^+ and $[MH - H_2O]^+$ ions are described by Pathways a–d. The reaction mechanisms ***m1–m18*** are summarized in Scheme 5).

Table 3. The nominal, measured and theoretical masses, mass measurement uncertainties (ppm), product ion identity and ion intensity for product ions observed in the IRMPD FTICR-MS experiments on STX[a]

Nominal	Measured	Calculated	ppm[b]	Formula	Intensity %
300[c]	300.14148	300.14143	+0.0	$C_{10}H_{18}N_7O_4^+$	
283	283.11493	283.11493	+0.0	$C_{10}H_{15}N_6O_4^+$	12
282	282.13093	282.13091	+0.1	$C_{10}H_{16}N_7O_3^+$	95
265	265.10441	265.10436	+0.2	$C_{10}H_{13}N_6O_3^+$	8
258	258.11969	258.11968	+0.0	$C_9H_{16}N_5O_4^+$	4
241	241.09314	241.09313	+0.0	$C_9H_{13}N_4O_4^+$	8
240	240.10912	240.10911	+0.0	$C_9H_{14}N_5O_3^+$	8
239	239.12504	239.12510	−0.3	$C_9H_{15}N_6O_2^+$	8
222	222.09850	222.09855	−0.2	$C_9H_{12}N_5O_2^+$	8
221	221.11454	221.11453	+0.0	$C_9H_{13}N_6O^+$	50
204	204.08797	204.08799	−0.3	$C_9H_{10}N_5O^+$	100
197	197.10334	197.10330	+0.2	$C_8H_{13}N_4O_2^+$	5
180	180.07674	180.07675	−0.1	$C_8H_{10}N_3O_2^+$	8
179	179.09273	179.09274	+0.0	$C_8H_{11}N_4O^+$	25
162	162.06622	162.06619	+0.2	$C_8H_8N_3O^+$	5
137	137.07101	137.07094	+0.5	$C_7H_9N_2O^+$	2

[a]Only those ions that were also observed in the triple-quadrupole CID spectra are listed here.
[b]Internally calibrated IRMPD spectra using the measured frequencies at *m/z* 175.11893 (y1), 246.15607 (y2), and 333.18807 (y3) of fragments of [Glu[1]]-Fibrinopeptide $[M + 2H]^{2+}$ ion (*m/z* 785.8) for calibration.
[c]Obtained from a separate internally calibrated FTICR full-scan experiment (see Experimental).

larly, for NEO, resolving powers in IRMPD MS/MS spectra ranged from 100,000 (*m/z* 298) to 217,000 (*m/z* 138).

Proton Affinities of STX and NEO

As mentioned above, STX and NEO exhibit two interesting structural features: (***a***) two guanidinium sites for potential proton attack per molecule; and (***b***) an opposite order of aqueous basicities of these two groups in NEO as compared to STX. For the elucidation of the dissociation pathways, it was crucial to find out if this trend was the same in the gas-phase. The influence of the −OH group at N-1 on basicity and the site of proton attack on the STX and NEO molecules was investigated by first examining the proton affinities of two simple model compounds, *N,N′*-trimethylguanidine, **1**, and its hydroxyl derivative, **2** (Scheme 4 and Table 5). When the B3LYP model (see Experimental) was applied to both molecules, the most susceptible position for proton attack was determined to be the imino nitrogen. Interestingly, the difference of *PA*(**1**) and *PA*(**2**) was very small, only 0.4 kcal·mol^{-1}, indicating that the −OH

Table 4. The nominal, measured and theoretical masses, mass measurement uncertainties (ppm), product ion identity, and ion intensity for product ions observed in the IRMPD FTICR-MS experiments on NEO[a]

Nominal	Measured	Calculated	ppm[b]	Formula	Intensity %
316[c]	316.13639	316.13639	+0.0	$C_{10}H_{18}N_7O_5^+$	
298	298.12573	298.12583	−0.2	$C_{10}H_{16}N_7O_4^+$	100
281	281.09919	281.09928	−0.3	$C_{10}H_{13}N_6O_4^+$	30
280	280.11501	280.11526	−0.9	$C_{10}H_{11}N_6O_3^+$	1
263	263.08866	263.08872	−0.2	$C_{10}H_{11}N_6O_3^+$	12
255	255.11987	255.12002	−0.5	$C_9H_{15}N_6O_3^+$	1
238	238.09342	238.09347	−0.2	$C_9H_{12}N_5O_3^+$	3
237	237.10942	237.10945	−0.1	$C_9H_{13}N_6O_2^+$	20
225	225.10941	225.10945	−0.2	$C_8H_{13}N_6O_2^+$	3
220	220.08285	220.08290	+0.2	$C_9H_{10}N_5O_2^+$	25
207	207.09885	207.09888	−0.2	$C_8H_{11}N_6O^+$	10
203	203.05629	203.05635	−0.3	$C_9H_7N_4O_2^+$	3
203	203.08013	203.08016	−0.2	$C_9H_9N_5O^{+\cdot}$	2
195	195.08762	195.08765	−0.2	$C_8H_{11}N_4O_2^+$	7
192	192.08791	192.08799	−0.4	$C_8H_{10}N_5O^+$	3
178	178.08489	178.08491	−0.1	$C_8H_{10}N_4O^{+\cdot}$	10
177	177.07707	177.07709	−0.1	$C_8H_9N_4O^+$	50
138	138.06619	138.06619	+0.0	$C_6H_8N_3O^+$	6

[a]Only those ions that were also observed in the triple-quadrupole CID spectra are listed here.
[b]Internally calibrated IRMPD spectra using the measured frequencies at *m/z* 175.11893 (y1), 246.15607 (y2), and 333.18807 (y3) of fragments of [Glu[1]]-Fibrinopeptide $[M + 2H]^{2+}$ ion (*m/z* 785.8) for calibration.
[c]Obtained from a separate internally calibrated FTICR full-scan experiment (see Experimental).

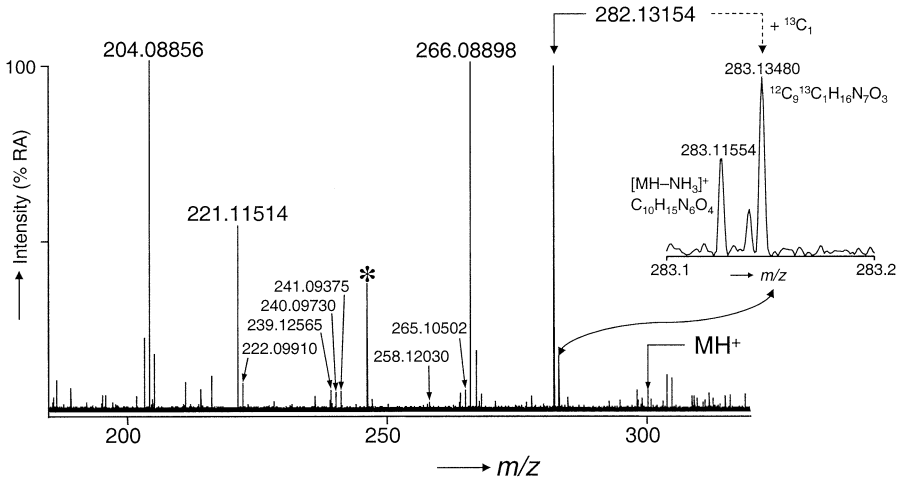

Figure 2. IRMPD/FTICR product ion spectrum of the MH^+ ion of STX and exact mass measurements for several important STX ions. The region around the $[MH - NH_3]^+$ ion is enlarged (asterisk denotes a Glu-Fib product ion).

group only slightly diminishes the proton affinity of **2** in comparison to **1**. Since the target compounds STX and NEO both possess carbamoyl groups at C-6 (Scheme 1), which can readily undergo intra-molecular hydrogen bonding, additional comparative calculations were carried out for two hypothetical molecules, **3** and **4**, in which the carbamoyl groups were replaced with $-CH_3$ to rule out intra-molecular hydrogen bonding effects (Scheme 4). It is important to emphasize that **3** and **4**, as shown in Scheme 4, represent the most stable forms of several possible tautomers. Their salient feature is that the five-membered imidazoline ring has the imino nitrogen within the ring (*endo*), whereas the amino group is attached in *exo* position to the ring. Protonation of **3** on either guanidinium group of the molecule ($\mathbf{3_L}$, $\mathbf{3_R}$) showed that $PA(\mathbf{3_L})$ (= 254.3 kcal·mol^{-1}) was significantly higher than $PA(\mathbf{3_R})$ (= 242.5 kcal·mol^{-1}), by ca. 12 kcal·mol^{-1}. In both cases, the calculations revealed that the proton attack occurred at the imino nitrogen. This was not surprising as imino nitrogen atoms are generally more basic than amino nitrogen atoms, as was observed in previous studies of guanidino derivatives [44–46]. The proton affinities for the two protonated species of **4** were similar; *viz.*, $PA(\mathbf{4_L})$ = 253.8 and $PA(\mathbf{4_R})$ = 240.6 kcal·mol^{-1}, indicating that the *PA*s were reduced by 0.5 and 1.9 kcal·mol^{-1} relative to the respective corresponding values of **3**. The difference in stability between the protonated species $\mathbf{4H^+L}$ and $\mathbf{4H^+R}$ was 13.2 kcal·mol^{-1} (Table 5).

In a similar manner, the structures of STX (**5**) and NEO (**6**) were investigated. The most stable structures of STX and NEO are shown in Scheme 4, with the intra-molecular hydrogen bonding indicated by dashed lines. The proton affinities $PA(\mathbf{5_L})$ and $PA(\mathbf{5_R})$ for STX were 257.7 and 250.2 kcal·mol^{-1}, respectively, indicating that the pyrimidine imino nitrogen is more basic in the gas-phase than the imidazoline imino nitrogen, similar to the behavior of **3**. The difference of $PA(\mathbf{5_L})$ and $PA(\mathbf{5_R})$ was 7.5 kcal·mol^{-1}, following the same basicity order as the p*K*a values in aqueous solution (p*K*a($\mathbf{5_L}$) = 11.5 and p*K*a($\mathbf{5_R}$) = 8.2; vide supra). Protonation of NEO (**6**) in the gas-phase gave similar results as compared to STX (**5**). The behavior, however, represented a reversal from the trend in the aqueous phase. The proton affinity $PA(\mathbf{6_L})$ = 254.0 kcal·mol^{-1} was higher than $PA(\mathbf{6_R})$ = 244.4 kcal·mol^{-1}, with a ΔPA of 9.6 kcal·mol^{-1}, in contrast to the observed p*K*a values in water [p*K*a($\mathbf{6_L}$) = 6.5, p*K*a($\mathbf{6_R}$) = 8.3]. We are currently investigating the physicochemical reasons for this trend reversal in solution-phase and gas-phase basicities, which will be discussed in a subsequent report. The important conclusion from the calculations was that the MH^+ precursor ion was protonated at the left guanidinium group for both STX and NEO, as demonstrated in the next section.

Dissociation Pathways and Mechanisms

The QqQ CID spectra (Figure 1) of STX and NEO were characterized by multiple consecutive losses of small neutrals from the MH^+ ion. The general fragmentation schemes in Schemes 2 and 3 are based on protonation at the left guanidinium group (see the discussion in the previous section). The corresponding fragmentation mechanisms for the observed reactions of STX and NEO comprised a combination of charge-remote and charge-mediated fragmentations, as summarized in Scheme 5. For the dissociation mechanisms, ***m1*** to ***m18***, refer to Schemes 2, 3, and 5.

There are a number of possible fragmentation possibilities for the MH^+ ions of STX and NEO. For example, after initial loss of H_2O from the ketone hydrate at C-12 (***m1***), the resulting ions at *m/z* 282 (STX) and 298 (NEO) readily underwent secondary neutral loss reactions of various small neutrals; NH_3 (***m2***, ***m7***), (CO_2 + NH_3) through a 6-centered concerted loss from the carbamoyl

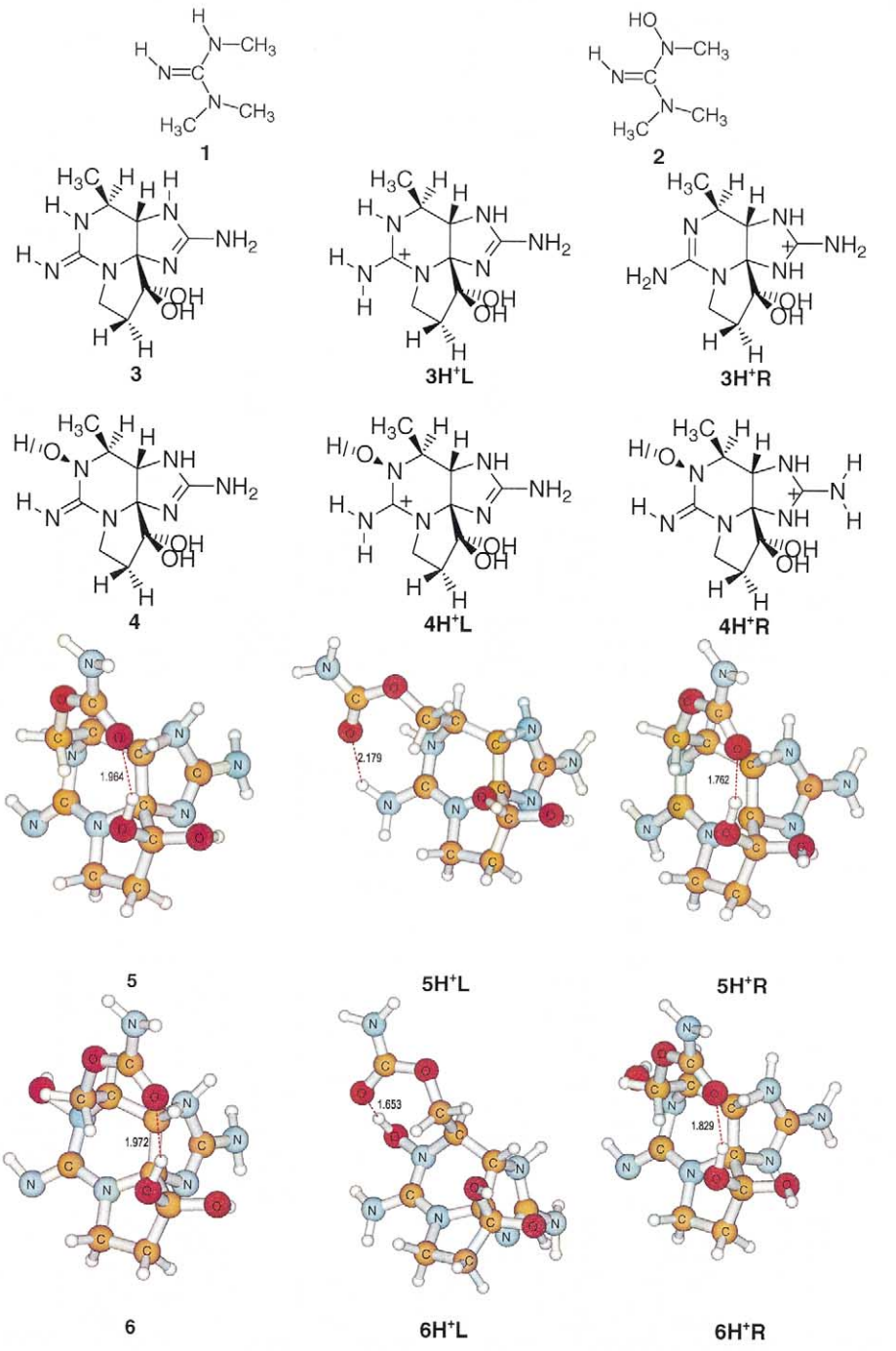

Scheme 4. Structures of the investigated protonated guanidinium species for proton affinity calculations (hydrogen bond distances [Å] are given for **5** and **6**).

group (***m3***), or HN=C=NH after opening of the imidazoline ring (***m5***). Third generation dissociation products were formed by expulsion of CO_2 after ring opening (***m4***) of the cyclic amide (formed via ***m2***), isocyanate cleavage NH=C=O (***m6***), or expulsion of other neutrals via ***m1***–***m3***, ***m5***, ***m7***, ***m9***, ***m11***, or ***m12***. The mechanisms of these reactions are detailed in Scheme **5**. Note that consecutive fragmentations reached up to six generations in the investigated *m/z* range between *m/z* 137 and 300/316 (Schemes **2** and **3**). Also, several of these reactions occurred in parallel from the MH^+ and subsequent product ions, as competing low-energy CID reactions. The initial parallel dissociations originating from MH^+ or from the dehydrated ion species are separated in Schemes **2a**–**d** and **3a**–**d**.

The following discussion focuses on two important

Table 5. The calculated proton affinities (*PA*) of the various investigated guanidinium species

Species (Scheme 4)	*PA* [kcal·mol^{-1}]
1	245.3
2	244.9
$\mathbf{3_L}$	254.3
$\mathbf{3_R}$	242.5
$\mathbf{4_L}$	253.8
$\mathbf{4_R}$	240.6
$\mathbf{5_L}$	257.7
$\mathbf{5_R}$	250.2
$\mathbf{6_L}$	254.0
$\mathbf{6_R}$	244.4

aspects of the fragmentation pattern: (1) differences between STX and NEO due to their dissimilar substitution pattern at N-1; and (2) differences originating from the ion activation techniques used in this study:

Differences between STX and NEO. There were several unique mechanisms in the dissociation pathways that either STX or NEO could or could not undergo because of the influence of the specific substitution pattern at N-1. STX, for example, exhibited a specific cleavage of NH_3 from *m/z* 258 (which originated via ***m5***) after going through a tautomeric transition state (***m8a***). The subsequent concerted loss of 61 u (CO_2 + NH_3, ***m3***) was specific to STX and was not observed for any later-generation NEO product ions. NEO showed a comparable, specific reaction, originating from *m/z* 220 (*220a*): after transfer of 2 hydrogens to give the tautomeric amino form at N-1, NH_3 was cleaved off at C-2 (***m8b***). In addition, NEO exhibited several further reactions involving the hydroxyl group at N-1 as one of the reaction centers, described by mechanisms ***m13***, ***m15***, and ***m18*** (vide infra).

Additionally, an interesting change from even-electron to odd-electron ions was observed for two later-generation product ions in the CID spectra of NEO. The ions at *m/z* 220 (*220b*, Scheme **3**) and *m/z* 195 (*195b*) cleaved off hydroxyl radicals from N-1 (***m15***) to give *m/z* 203 (*203b*) and *m/z* 178, as confirmed by their exact masses in IRMPD (Table 4). The corresponding ions in the STX spectrum at *m/z* 204 (*204a*) and *m/z* 179 (Scheme **2**) therefore did not exhibit comparable radical ·OH losses, as STX does not have a hydroxyl group at N-1. Similar even-electron to odd-electron switches at higher stages of MS^n were observed by Strife and coworkers [52] in their analysis of morphinane derivatives because the corresponding species lacked other favorable fragmentation pathways. Interestingly, the NEO species *237b* and *195b* can further rearrange to *237a* or *195a* via hydroxyl transfer from N-1 to C-13 (***m13***; Schemes **3b** and **5**). These rearrangements were followed by loss of either CH_2O (***m16***) or water (***m14***) to yield *m/z* 207 and 177, respectively. There was one further reaction unique to NEO that resulted from consecutive fragmentation following a NEO-specific cleavage; the formation of *m/z* 192 (*192b*) via expulsion of CO (***m17***) from *m/z* 220 (*220b*).

Differences between the ion activation techniques. There were a few noteworthy differences between CID and IRMPD. For example, while all three MS/MS techniques formed abundant first generation $[MH - H_2O]^+$ ions (STX: *m/z* 282; NEO: *m/z* 298), the product ion at *m/z* 283 in the spectra of STX (loss of NH_3 from the MH^+ ion; see expanded region of Figure 2) was observed with a significant abundance only in the IRMPD and IT MS^2 spectra. QqQ CID formed this ion only to an insignificant amount or it was just a short-lived unstable intermediate. Furthermore, the two-fold loss of NH_3 from the MH^+ ion of STX yielded one of the most abundant ions in the IRMPD spectrum (*m/z* 266; Figure 2) and it was also a major ion in the IT MS^2 spectrum of *m/z* 300 (Table 1). It was not, however, observed in the QqQ CID spectrum (Figure 1a). It appears that the ion activation by IRMPD and IT CID favored the initial losses of NH_3 in comparison to the triple-quadrupole instrument. Consequently, the STX ion species at *m/z* 205 in IRMPD and MS^n due to a 61 u loss from *m/z* 266 (concerted CO_2/NH_3 cleavage, ***m3***) was naturally absent in the QqQ CID spectra, while it formed the base peak in the IT MS^3 spectrum ($300^+ \rightarrow 266^+ \rightarrow 205^+$). A similar behavior was obtained for NEO only in IRMPD, but no ions due to the initial NH_3 losses were observed in the IT MS^2 analysis.

Another interesting observation was made for the intense product ions at *m/z* 148 (STX) and *m/z* 164 (NEO) in the QqQ CID spectra (Figure 1; Schemes **2** and **3**). Both products were confirmed as being formed from *m/z* 204 (STX) and *m/z* 220 (NEO), respectively, from IT MS^3 (STX: $300^+ \rightarrow 204^+ \rightarrow 148^+$; NEO: $316^+ \rightarrow 220^+ \rightarrow 164^+$) and IT MS^4 (STX: $300^+ \rightarrow 282^+ \rightarrow 204^+ \rightarrow 148^+$; NEO: $316^+ \rightarrow 298^+ \rightarrow 220^+ \rightarrow 164^+$) experiments (Tables 1, 2). As neither ion was observed in the IRMPD analyses, their identities could not be finally confirmed by their exact masses. The loss of 56 u from *m/z* 204 and 220 and the fact that they form the base peaks in the respective IT MS^3 and MS^4 spectra suggest that they originate from loss of cyclopropanone (C_3H_4O, ***m10***), as proposed in Schemes **2**, **3**, and **5**.

In general, the relative ion abundances in the QqQ CID and IRMPD spectra correlated very well for most product ions such as *m/z* 282, 221, 204, 180, and 179 (Figures 1, 2), but differed significantly for a few others such as *m/z* 283 and 266 (vide supra). Another poor correlation between IRMPD and CID was observed for the product ion at *m/z* 138, which represented a major ion in the QqQ spectra of both STX and NEO (Figure 1; Schemes **2** and **3**). This ion was formed by loss of a ketenimine from *m/z* 179 (STX) and *m/z* 195 (195b) via ***m9***. IRMPD of NEO's MH^+ ion, however, generated *m/z* 138 only to a small extend (Table 4); it was not observed at all in the IRMPD spectrum of STX.

Fragmentation Pathway	Loss	Mechanism
m1	H_2O	
m2	NH_3	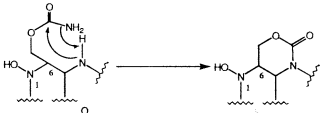
m3	CO_2, NH_3	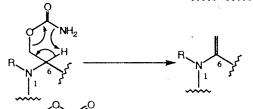
m4	CO_2	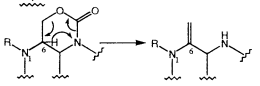
m5	HN=C=NH	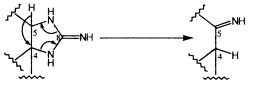
m6	O=C=NH	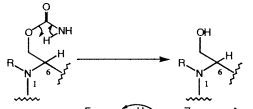
m7	NH_3	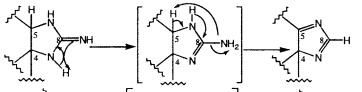
m8a	NH_3	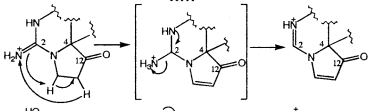
m8b	NH_3	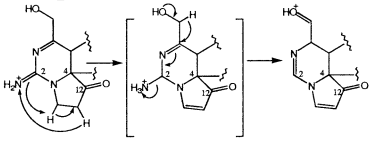

Fragmentation Pathway	Loss	Mechanism
m9	$H_2C=C=NR$ (R=H/OH)	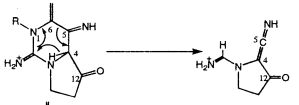
m10	C_3H_4O	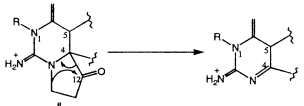
m11	NH=C=NR (R=H/OH)	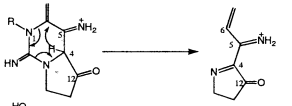
m12	H_2O	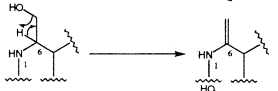
m13	rearrangement	
m14	H_2O	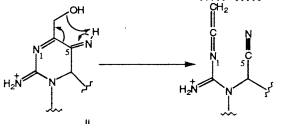
m15	$OH^{\bullet}$	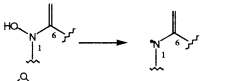
m16	CH_2O	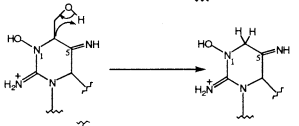
m17	CO	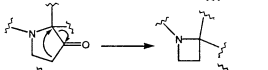
m18	H_2O	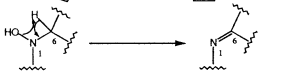

Scheme 5. Proposed principal dissociation mechanisms for STX and NEO (the numbering scheme ***m1*** to ***m18*** refer to reactions in Schemes **2** and **3**).

Conclusions

The gas-phase dissociation pathways of two paralytic shellfish poisons (PSPs), saxitoxin (STX) and neosaxitoxin (NEO), were investigated in this study. Structural studies on these poisons are important for both analytical characterization of the highly toxic PSPs and for identification of yet unknown toxins. The product ion mass spectra of the PSPs exhibited an unusually rich variety and abundance of species due to the large number of functional groups within the small skeletal structures and the two guanidinium moieties per molecule. A comprehensive approach to structural elucidation was successfully carried out. Starting with triple-quadrupole product ion spectra as templates, linked ion-trap MS^n data were added to provide tentative dissociation schemes. Subsequent high-resolution FTICR analysis provided the exact mass data and elemental formulae for confirming the identity of the product ions. This particular combination of instruments allowed the rapid generation of the bulk of the required data via automated procedures on the triple-quadrupole and ion-trap instruments. While FTICR instruments are inherently slower, the infrared multiphoton dissociation (IRMPD) "shotgun" approach taken here matched the speed of the other procedures because it can generate all required product ions in just one IRMPD experiment per PSP toxin. New commercial instrument designs such as quadrupole linear ion-trap or hybrid quadrupole linear ion-trap/FTICR can accelerate the process by combining some of the described experiments.

The actual dissociation mechanisms of the PSPs were proposed after calculations of proton affinities revealed that protonation took place at the pyrimidine guanidinium moieties of both STX and NEO. Most of the parallel and consecutive dissociation reactions could then be rationalized through charge-remote and charge-mediated multiple neutral losses of H_2O, NH_3, CO, CO_2, CH_2O and different isocyanate, ketenimine and diimine species. The high degree of similarity between many of the pathways of STX and NEO will undoubtedly help characterize the chemical structures of other PSPs. For example, the related gonyautoxins are expected to show similar fragmentation patterns as shown in this report. Furthermore, some of the described product ions are of a generic nature and could be used for screening assays or rapid discovery of new analogs and biotransformation products.

Acknowledgments

The authors thank Dr. Alan Marshall and Dr. Michael Chalmers (NHMFL, Tallahassee, Florida) for helpful discussions and Dr. Stephan Brombacher (NRC/IMB, Halifax) for help with the ion-trap experiments. This work was supported in part by the NSF National High-Field FTICR-MS Facility, CHE-99–09052. LS acknowledges financial assistance received from le Fonds Québecois de la recherche sur la nature et les technologies (FCAR) and the NRC's Graduate Student Scholarship Supplement Program (GSSSP).

References

1. Luckas, B. Phycotoxins in Seafood—Toxicological and Chromatographic Aspects. *J. Chromatogr.* **1992,** *624,* 439–456.
2. Hallegraeff, G. M. A Review of Harmful Algal Blooms and Their Apparent Global Increase. *Phycologia* **1993,** *32,* 79–99.
3. Van Egmond, H. P.; Aune, T.; Lassus, P.; Speijers, G. J. A.; Waldock, M. Paralytic and Diarrhetic Shellfish Poisons. Occurrence in Europe, Toxicity, Analysis, and Regulation. *J. Nat. Toxins* **1993,** *2,* 41–83.
4. Favre, I.; Moczydlowski, E.; Schild, L. Specificity for Block by Saxitoxin and Divalent Cations at a Residue which Determines Sensitivity of Sodium Channel Subtypes to Guanidinium Toxins. *J. Gen. Physiol.* **1995,** *106,* 203–229.
5. Hille, B. An Essential Ionized Acid Group in Sodium Channels. *Fed. Proc.* **1975,** *34,* 1318–1321.
6. Spalding, B. C. Properties of Toxin-Resistant Sodium Channels Produced by Chemical Modification in Frog Skeletal Muscle. *J. Physiol.* **1980,** *305,* 485–500.
7. Sakamoto, Y.; Lockey, R. F.; Krzanoswski, J. R. Shellfish and Fish Poisoning Related to the Toxic Dinoflagellates. *S. Med. J.* **1987,** *80,* 866–872.
8. De Carvalho, M.; Jacinto, J.; Ramos, N.; de Oliveira, V.; Pinho e Melo, T.; de Sa, J. Paralytic Shellfish Poisoning: Clinical and Electrophysiological Observations. *J. Neurol.* **1998,** *245,* 551–554.
9. Llewellyn, L. E.; Dodd, M. J.; Robertson, A.; Ericson, G.; de Koning, C.; Negri, A. P. Post-Mortem Analysis of Samples from a Human Victim of a Fatal Poisoning Caused by the Xanthid Crab, Zosimus aeneus. *Toxicon* **2002,** *40,* 1463–1469.
10. Shimizu, Y.; Hsu, C. P.; Fallon, W. E.; Oshima, Y.; Miura, I.; Nakanishi, K. Structure of Neosaxitoxin. *J. Am. Chem. Soc.* **1978,** *100,* 6791–6793.
11. Boyer, G. L.; Schantz, E. J.; Schnoes, H. K. Characterization of 11-Hydroxysaxitoxin Sulphate, a Major Toxin in Scallops Exposed to Blooms of the Poisonous Dinoflagellate. *J. Chem. Soc. Chem. Commun.* **1978**, 889–890.
12. Shimizu, Y. The Chemistry of Paralytic Shellfish Toxins. *Marine Toxins and Venoms;* In: Tu, A. T., Ed.; Marcel Dekker: New York, 1988; p. 63.
13. Van Egmond, H. P.; van den Top, H. J.; Paulsch, W. E.; Gonega, X.; Vieytes, M. R. Paralytic Shellfish Poison Reference Materials: An Intercomparison of Methods for the Determination of Saxitoxin. *Food Add. Contam.* **1994,** *11,* 39–56.
14. Krogh, P. Measurements of Paralytic Shellfish Poisons. *Nord. Vet. Med.* **1979,** *31,* 302–308.
15. Quilliam, M. A. Liquid Chromatography-Mass Spectrometry of Seafood Toxins. *In Applications of LC-MS in Environmental Chemistry;* Barcelo, D., Ed.; Elsevier: Amsterdam, 1996; p 415.
16. Quilliam, M. A.; Hess, P.; Dell'Aversano, C. Recent Developments in the Analysis of Phycotoxins by Liquid Chromatography-Mass Spectrometry. *Mycotoxins and Phycotoxins in Perspective at the Turn of the Century*. May, 2000, pp 383-391. In: DeKoe, W. J.; Samson, R. A.; Van Egmond, H. P.; Gilbert, J.; Sabino, M., Eds.; *Proceedings of the 10th International IUPAC Symposium Mycotoxins Phycotoxins*; Sao Paulo, Brazil.
17. Quilliam, M. A. The Role of Chromatography in the Hunt for Red Tide Toxins. *J. Chromatogr. A* **2003,** *1000,* 527–548.
18. Thibault, P.; Pleasance, S.; Laycock, M. V. Analysis of Paralytic Shellfish Poisons by Capillary Electrophoresis. *J. Chromatogr.* **1991,** *542,* 483–501.
19. Kawatsu, K.; Hamano, Y.; Sugiyama, A.; Hashizume, K.; Noguchi, T. Development and Application of an Enzyme Immunoassay Based on a Monoclonal Antibody Against Gonyautoxin Components of Paralytic Shellfish Poisoning Toxins. *J. Food Prot.* **2002,** *65,* 1304–1308.
20. Sphon, J. Use of Mass Spectrometry for Confirmation of Animal Drug Residues. *J. Assoc. Off. Anal. Chem.* **1978,** *6,* 1247.

21. Nakamura, M.; Oshima, Y.; Yasumoto, T. Occurrence of Saxitoxin in Pufferfish. *Toxicon* **1984,** *22,* 381–385.
22. White, K. D.; Sphon, J. A.; Hall, S. Fast Atom Bombardment Mass Spectrometry of 12 Marine Toxins Isolated from Protogonyaula. *Anal. Chem.* **1986,** *58,* 562–565.
23. Mirocha, C. J.; Cheong, W.; Mirza, U.; Kim, Y. B. Analysis of Saxitoxin in Urine by Continuous-Flow Fast Atom Bombardment Mass Spectrometry. *Rapid Commun. Mass Spectrom.* **1992,** *6,* 128–134.
24. Quilliam, M. A.; Janecek, M.; Lawrence, J. F. Characterization of the Oxidation Products of Paralytic Shellfish Poisoning Toxins by Liquid Chromatography/Mass Spectrometry. *Rapid Commun. Mass Spectrom.* **1993,** *7,* 482–487.
25. Dahlmann, J.; Budakoswski, W. R.; Luckas, B. Liquid Chromatography-Electrospray Ionization Mass Spectrometry Based Methods for the Simultaneous Determination of Algal and Cyanobacterial Toxins in Phytoplankton from Marine Waters and Lakes Followed by Tentative Structural Elucidation of Microcystins. *J. Chromatogr. A* **2003,** *994,* 45–57.
26. Arakawa, O.; Noguchi, T.; Shida, Y.; Onoue, Y. Occurrence of Carbamoyl-N-Hydroxy Derivatives of Saxitoxin and Neosaxitoxin in a Xanthid Crab Zosimus aeneus. *Toxicon* **1994,** *32,* 175–183.
27. Pleasance, S.; Thibault, P.; Kelly, J. Comparison of Liquid-Junction and Coaxial Interfaces for Capillary Electrophoresis-Mass Spectrometry with Application to Compounds of Concern to the Aquaculture Industry. *J. Chromatogr.* **1992,** *591,* 325–339.
28. Hashimoto, T.; Nishio, S.; Nishibori, N.; Yoshioka, S.; Noguchi, T. A New Analytical Method for Gonyautoxins Based on Postcolumn HPLC. *J. Food Hyg. Soc. Japan* **2002,** *43*(144), 147.
29. Andrinolo, D.; Michea, L. F.; Lagos, N. Toxic Effects, Pharmacokinetics, and Clearance of Saxitoxin, a Component of Paralytic Shellfish Poison (PSP), in Cats. *Toxicon* **1999,** *37,* 447–464.
30. Wils, E. R. J.; Hulst, A. G. Determination of Saxitoxin by Liquid Chromatography/Thermospray-Mass Spectrometry. *Rapid Commun. Mass Spectrom.* **1993,** *7,* 413–415.
31. Pleasance, S.; Ayer, S. W.; Laycock, M. V.; Thibault, P. Ionspray Mass Spectrometry of Marine Toxins. III. Analysis of Paralytic Shellfish Poisoning Toxins by Flow-Injection Analysis, Liquid Chromatography/Mass Spectrometry, and Capillary Electrophoresis/Mass Spectrometry. *Rapid Commun. Mass Spectrom.* **1992,** *6,* 14–24.
32. Buzy, A.; Thibault, P.; Laycock, M. V. Development of a Capillary Electrophoresis Method for the Characterization of Enzymatic Products Arising from the Carbamoylase Digestion of Paralytic Shellfish Poisoning Toxins. *J. Chromatogr.* **1994,** *688,* 301–316.
33. Locke, S. J.; Thibault, P. Improvement in Detection Limits for the Determination of Paralytic Shellfish Poisoning Toxins in Shellfish Tissues Using Capillary Electrophoresis/Electrospray Mass Spectrometry and Discontinuous Buffer Systems. *Anal. Chem.* **1994,** *66,* 3436–3446.
34. Quilliam, M. A.; Thomson, B. A.; Scott, G. J.; Siu, K. W. M. Ion Spray Mass Spectrometry of Marine Neurotoxins. *Rapid Commun. Mass Spectrom.* **1989,** *3,* 145–150.
35. Reyero, M.; Cacho, E.; Martinez, A.; Vazquez, J.; Marina, A.; Fraga, S.; Franco, J. M. Evidence of Saxitoxin Derivatives as Causative Agents in the 1997 Mass Mortality of Monk Seals in the Cape Blanc Peninsula. *Nat. Toxins* **1999,** *7,* 311–315.
36. Ito, K.; Asakawa, M.; Sida, Y.; Miyazawa, K. Occurrence of Paralytic Shellfish Poison (PSP) in the Starfish Asterina pectinifera Collected from the Kure Bay, Hiroshima Prefecture, Japan. *Toxicon* **2003,** *41,* 291–295.
37. Chowdhury, S. K.; Katta, V.; Chait, B. T. An Electrospray Ionization Mass Spectrometer with New Features. *Rapid Commun. Mass Spectrom.* **1990,** *4,* 81–87.
38. Wilcox, B. E.; Hendrickson, C. L.; Marshall, A. G. Improved Ion Extraction From a Linear Octopole Ion Trap: SIMION Analysis and Experimental Demonstration. *J. Am. Soc. Mass Spectrom.* **2002,** *11,* 1304–1312.
39. Marshall, A. G.; Verdun, F. R. Fourier Transforms in NMR, Optimal, and Mass Spectrometry: A User's Handbook; Elsevier: Amsterdam, 1990, p 80.
40. Shi, S. D.-H.; Drader, J. J.; Freitas, M. A.; Hendrickson, C. L.; Marshall, A. G. Comparison and Interconversion of the Two Most Common Frequency-to-Mass Calibration Functions for Fourier Transform Ion Cyclotron Resonance Mass Spectrometry. *Int. J. Mass Spectrom* **2000,** *195/196,* 591–598.
41. Ledford, E. B.; Rempel, D. L.; Gross, M. L. Space Charge Effects in Fourier Transform Mass Spectrometry. Mass Calibration. *Anal. Chem.* **1984,** *56,* 2744–2748.
42. Marshall, A. G.; Wang, T.-C. L.; Ricca, T. L. Tailored Excitation for Fourier Transform Ion Cyclotron Mass Spectrometry. *J. Am. Chem. Soc.* **1985,** *107,* 7893–7897.
43. Guan, S.; Marshall, A. G. Stored Waveform Inverse Fourier Transform (SWIFT) Ion Excitation in Trapped-ion Mass Spectrometry: Theory and Applications. *Int. J. Mass Spectrom. Ion Processes* **1996,** *157/158,* 5–37.
44. Maksić, Z.B.; Kovačević, B. Absolute Proton Affinity of Some Polyguanides. *J. Org. Chem.* **2000,** *65,* 3303–3309.
45. Kovačević, B.; Maksić, Z. B.; Vianello, R. The Proton Affinity of Some Extended π-Systems Involving Guanidine and Cyclopropenimine Subunits. *J. Chem Soc. Perkin Trans. 2* **2001,** 886–891.
46. Vianello, R.; Kovačević, B.; Maksić, Z. B. In Search of Neutral Organic Superbases—Iminopolyenes and Their Amino Derivatives. *New J. Chem.* **2002,** *26,* 1324–1328.
47. Koch, W; Holthausen, M. C. A Chemist Guide to Density Functional Theory; Wiley-VCH: Weinheim/New York, 2000, and references cited therein.
48. Alcami, M.; Mó, O.; Yañez, M. Computational Chemistry: A Useful (Sometimes Mandatory) Tool in Mass Spectrometry Studies. *Mass Spectrom. Rev.* **2001,** *20,* 195–245 and references cited therein..
49. Frisch, M. J.; Trucks, G. W.; Schlegel, H. B.; Scuseria, G. E.; Robb, M. A.; Cheeseman, J. R.; Zakrzewski, V. G.; Montgomery, J. A., Jr.; Stratmann, R. E.; Burant, J. C.; Dapprich, S.; Millam, J. M.; Daniels, A. D.; Kudin, K. N.; Strain, M. C.; Farkas, O.; Tomasi, J.; Barone, V.; Cossi, M.; Cammi, R.; Mennucci, B.; Pomelli, C.; Adamo, C.; Clifford, S.; Ochterski, J.; Petersson, G. A.; Ayala, P. Y.; Cui, Q.; Morokuma, K.; Malick, D. K.; Rabuck, A. D.; Raghavachari, K.; Foresman, J. B.; Cioslowski, J.; Ortiz, J. V.; Baboul, A. G.; Stefanov, B. B.; Liu, G.; Liashenko, A.; Piskorz, P.; Komaromi, I.; Gomperts, R.; Martin, R. L.; Fox, D. J.; Keith, T.; Al-Laham, M. A.; Peng, C. Y.; Nanayakkara, A.; Gonzalez, C.; Challacombe, M.; Gill, P. M. W.; Johnson, B. G.; Chen, W.; Wong, M. W.; Andres, J. L.; Head-Gordon, M.; Replogle, E. S.; Pople, J. A. Gaussian 98 Rev A 10; Gaussian, Inc.: Pittsburgh, PA, 1998.
50. Shimizu, Y. Paralytic Shellfish Poisons. *In Progress in the Chemistry of Organic Natural Products;* Herz, W.; Grisebach, H.; Kirby, G. W., Eds.; Springer: New York, 1984; pp 235–264.
51. Rogers, R. S.; Rapoport, H. The pKa's of Saxitoxin. *J. Am. Chem. Soc.* **1980,** *102,* 7335–7339.
52. Strife, R. J.; Robosky, L. C.; Garret, G.; Ketcha, M. M.; Shaffer, J. D.; Zhang, N. Ion Trap MS^n Genealogical Mapping—Approaches for Structure Elucidation of Novel Products of Consecutive Fragmentations of Morphinans. *Rapid Commun. Mass Spectrom.* **2000,** *14,* 250–260.
53. Xie, Y.; Lebrilla, C. B. Infrared Multiphoton Dissociation of Alkali Metal-Coordinated Oligosaccarides. *Anal. Chem.* **2003,** *75,* 1590–1598.